Preface:
Metamorphism and Orogenic Belts—Response from Micro- to Macro-Scale

Xu-Ping Li[1], Hans-Peter Schertl[2,3], Jürgen Reinhardt[4,3]

1. *Shandong Key Laboratory of Depositional Mineralization and Sedimentary Minerals, Shandong University of Science and Technology, Qingdao 266590, China*
2. *Ruhr-University Bochum, Institute of Geology, Mineralogy and Geophysics, D-44780 Bochum, Germany*
3. *College of Earth Science and Engineering, Shandong University of Science and Technology, Qingdao 266590, China*
4. *Department of Earth Sciences, University of the Western Cape, Bellville 7535, South Africa*

ABSTRACT: The geological toolbox for the analysis of orogenic processes has seen substantial additions over the recent decades. Major advances have been made in the ability to simulate geological conditions and processes by computer modeling, we have a much improved knowledge of geochemical processes (trace elements and isotopes in particular), and, last but not least, the range and versatility of micro-analytical methods and instrumentation available to us has been expanded dramatically. The latter aspect has had a particular impact on metamorphic petrology as the conventional tools to determine pressure-temperature-time paths via rock and mineral analysis combined with isotope geochronology have generally gained in precision and accuracy through a much improved resolution. Geochronology has moved from whole-grain analysis to spot analyses on zoned single grains while analyzing trace elements and isotopes at the same time. It is therefore possible to recognize complex multi-stage orogenic events in single samples or single grains. Diffusion profiles in minerals provide us with time-scales of metamorphic and magmatic processes. Major and trace elements as well as isotope profiles of mineral grains give us insight into changing ambient conditions during mineral growth. This special issue focuses on pressure-temperature conditions and geochronology of metamorphic rocks, isotope studies of magmatic rocks, partial melting and metasomatic processes, all with a view at tectonic implications and orogeny. Much of the evidence has been gained from small-scale observation and analysis. Diligent field work and detailed microscopic examination remain indispensable, though, as demonstrated clearly by the "expansion" of the *P-T* space as applicable to crustal metamorphic processes towards extreme pressures and temperatures. As a consequence, much interest has thus focused on UHP and UHT rocks and the orogenic processes that generate them. There is petrological evidence for subduction to, and subsequent exhumation from, depths in excess of 250 km. While this impacts substantially on the large-scale geodynamic models of orogenic processes, the evidence is gathered primarily from small-scale petrological observation. The same applies in principle to UHT granulites. To generate temperatures in the 900 to 1 100 °C range within the sillimanite stability field in orogenic heat budget models remains a serious challenge, however. The large overlap of solid-state metamorphism, partial anatexis and magmatic crystallization in *P-T* space suggests close interrelationships, and the role and contribution of the diverse magmatic activities in forming orogenic belts, from the onset of subduction to late-orogenic delamination or slab-break-off is crucial for our understanding of geodynamics, with focus on geochemistry and geochronology. Aspects of metasomatism in the framework of orogeny are given some special consideration in this issue. The topics include the formation of sagvandite, pyrope quartzite (or whiteschist), jadeitite and rodingite. One of the key questions addressed is the source and the nature of the fluids that triggered the different types of metasomatic events. Finally, it is shown how small-scale methods contribute to a better understanding of the formation of deep-seated mantle xenoliths.

KEY WORDS: orogeny, metasomatism, UHP metamorphism, UHT metamorphism, geochemistry, geochronology.

0 INTRODUCTION

Orogenic belts are formed in a range of geodynamic environments and are commonly considered to be a result of plate tectonics, with the exception of the "pre-plate-tectonic era" (>3 Ga). The current issue is related to a broad spectrum of processes that contribute to, or result from, the formation of orogens. Due to the diversity of such processes producing magmatic, metamorphic and metasomatic rocks, the topics involved and presented here vary widely. This issue contains papers that focus on age dating

and isotope studies of magmatic rocks, pressure-temperature conditions and geochronological studies of metamorphic rocks and respective tectonic implications, partial melting and metasomatic processes, as well as on small-scale observations.

1   FORMATION OF OROGENS IN GENERAL

Some fundamental questions to be asked are: What kind of processes contribute to the formation of orogens and what is their spatial extent? What are the major types of orogens in the broadest sense, and how do they relate to plate tectonic settings and mechanisms?

Key areas of the formation of orogens are convergent plate boundaries. Complex mechanisms occur when the oceanic lithosphere subsides and becomes subducted below continental lithosphere. Typically, within such subduction zone settings blueschist and eclogite are formed. Water stored in pre-subduction oceanic crust from sub-seafloor metamorphism and in the sediments that were deposited on this crust will be released during subduction-related dehydration processes, triggering the formation of melts and hydration (serpentinization) of originally dry mantle-derived rocks. Fluids rich in H_2O and/or CO_2 released from the subducting slab are also known to cause mantle metasomatism in the mantle wedge of the upper-plate margin. Subduction zones as those of the Andes in South America are characterized by an intense magmatic activity. Basaltic melts which underwent contamination and assimilation processes (and to a minor extent also magma mixing) during ascent, led to the development of a volcanic chain of more than 7 000 km in length, essentially consisting of andesitic volcanoes. Due to anatectic processes, mainly within the continental crust, but also within oceanic crust, and due to differentiation processes of basaltic melts, granitic melts can be produced.

Continent-continent collision typically starts with the closure of the ocean between converging continents and hence the change from oceanic lithosphere subduction to continental subduction, the latter being limited in extent by the buoyancy of the thickened crust. Two relatively young examples of such collision zones are the Himalayas which resulted from the collision of the Indian subcontinent with the Eurasian Plate, and the European Alps which were formed when the African and Eurasian plates were colliding. The particular significance of ophiolites is well demonstrated in these two orogens, being the remnants of the pre-collisional oceanic lithosphere, thus marking the suture zone between the converging plates as well as giving insight into subduction or exhumation processes. During continent-continent collision, deep subduction may lead to the formation of ultrahigh-pressure (UHP) metamorphic rocks (see Section 2). Collisional processes may also be accompanied by the formation of different types of magma as well as the formation of UHT metamorphic rocks (see Section 2).

If two oceanic plates are colliding at convergent margins, one oceanic plate will become subducted below the other and island arc orogens can form. The magmatic rocks forming these islands can only derive from the oceanic crust or the mantle below and are typically of tholeiitic character. Differentiation processes may lead to very small amounts of granitoids.

The current issue represents a compilation of papers which documents how small-scale observations in magmatic, metamorphic and metasomatic rocks contribute to a better understanding on how orogens develop.

2   THE ROLE OF METAMORPHISM

Until the early 1980s it was generally believed that the maximum pressures metamorphic rocks experienced did not exceed about 12 kbar, which equals a thickness of the continental crust of about 40 km. Thus, classical textbooks in geosciences typically show pressure-temperature (*P-T*) diagrams that do not go beyond 10–12 kbar. The upper temperature limit displayed is usually 800–1 000 ºC.

The discovery of coesite (Fig. 1a) in metamorphic rocks from the Dora-Maira Massif, northern Italy (Chopin, 1984), and the Western Gneiss Region, Norway (Smith, 1984) revolutionized metamorphic petrology as well as the studies of crustal dynamics. The pressure-temperature range that reflects metamorphic reactions occurring in natural rocks expanded to pressures of at least around 30 kbar. A couple of years later metamorphic diamond was discovered in the Kokchetav Massif (Kazakhstan), which demonstrated that pressures of about 40 kbar must have been reached during subduction and related metamorphism of continental crust (Sobolev and Shatsky, 1990). The search for higher pressures did continue further, and the discovery of clinopyroxene exsolution in garnet followed, which is seen as evidence for a former majorite component. This means, that at pressures in the diamond stability field, garnet contains not only Si in 4-fold but also in 6-fold coordination, leading to a hypothetical end member composition of $Mg_3MgSi^{[6]}[Si^{[4]}O_4]_3$. Further UHP indicators reported in the literature are α-PbO_2-type TiO_2, and even the possibility of quartz pseudomorphs after stishovite is discussed (Kojitani et al., 2018; Liu et al., 2007) which would require minimum pressures of 80 kbar, corresponding to a subduction to depths of at least 300 km (Fig. 2) as well as exhumation processes operating over such vertical distances to get the rocks to the surface.

Following the discovery of coesite the term ultrahigh-pressure (UHP) metamorphism was established in the literature, which refers to pressure conditions above the quartz stability field. The occurrence of UHP-rocks in 1984 (Chopin, 1984; Smith, 1984) was—at that time—interpreted as an exotic case of deep subduction of crustal rocks to mantle depths, but it also triggered an intense search for further UHP localities. Meanwhile more than 20 occurrences worldwide, some of which have an extent of more than 1 000 km in length, demonstrate that the formation of UHP metamorphic rocks during subduction/collision-related processes is far more common than previously assumed. Classical regions of UHP-metamorphism are the Dora-Maira Massif (Italy), the Kokchetav Massif (Kazakhstan), the Rhodopes (Greek-Bulgarian border), the Erzgebirge (Germany), the Western Gneiss Region (Norway), the Dabie Mountains and Sulu Orogen as well as North Qaidam (China), and Tso Morari (Himalaya). Typical UHP-related reactions and stability fields are shown in Fig. 2.

With respect to metamorphic temperatures, granulites represent rocks that experienced a metamorphic overprint higher than 650 (at low *P*) to 800 ºC (at higher *P*). Already in the 1970s evidence had been published that some crustal rocks experienced metamorphic conditions exceeding 1 000 ºC (Morse and Talley,
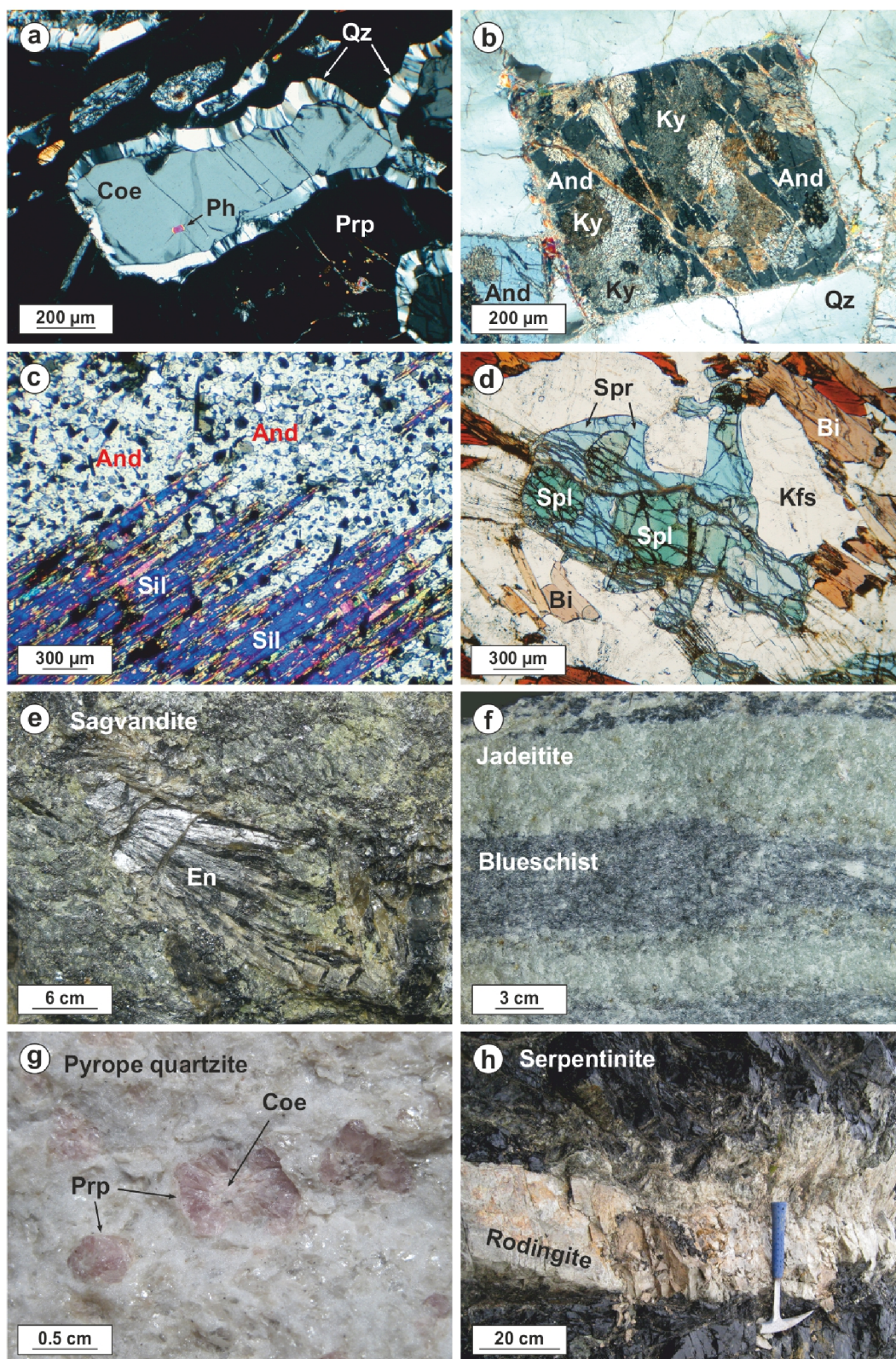
Figure 1. Photomicrographs of typical HP-UHP and HT-UHT associations (a)–(d), and a suite of typical metasomatic rock samples (e)–(h) covered in this special issue. (a) Coesite inclusion surrounded by palisade-textured secondary quartz in pyrope (Dora-Maira Massif, Italy), crossed polarized (XPL); (b) paramorphic transformation of andalusite to kyanite (Eisenalm, Kreuzeckgruppe, Carinthia, Austria), XPL; (c) topotaxial paramorphic replacement of andalusite by sillimanite (Mary Kathleen Fold Belt, NE Australia), XPL; (d) green spinel surrounded by sapphirine in granulite (~4 km NW Shaerqin, Inner Mongolia), plane-polarized light (PPL); (e) sagvandite with spray of enstatite crystals, Norway (c.f., Bucher and Stober, 2019); (f) jadeitite and blueschist country rock, Rio San Juan Complex, Dominican Republic; and (g) pyrope quartzite, Dora-Maira Massif, Italy with a coesite inclusion in pyrope (c.f., Schertl et al., 2019); (h) rodingite vein in serpentinite (Purang ophiolite, western Tibet, China; c.f., Wang et al., 2019). Mineral abbreviations after Whitney and Evans (2010).
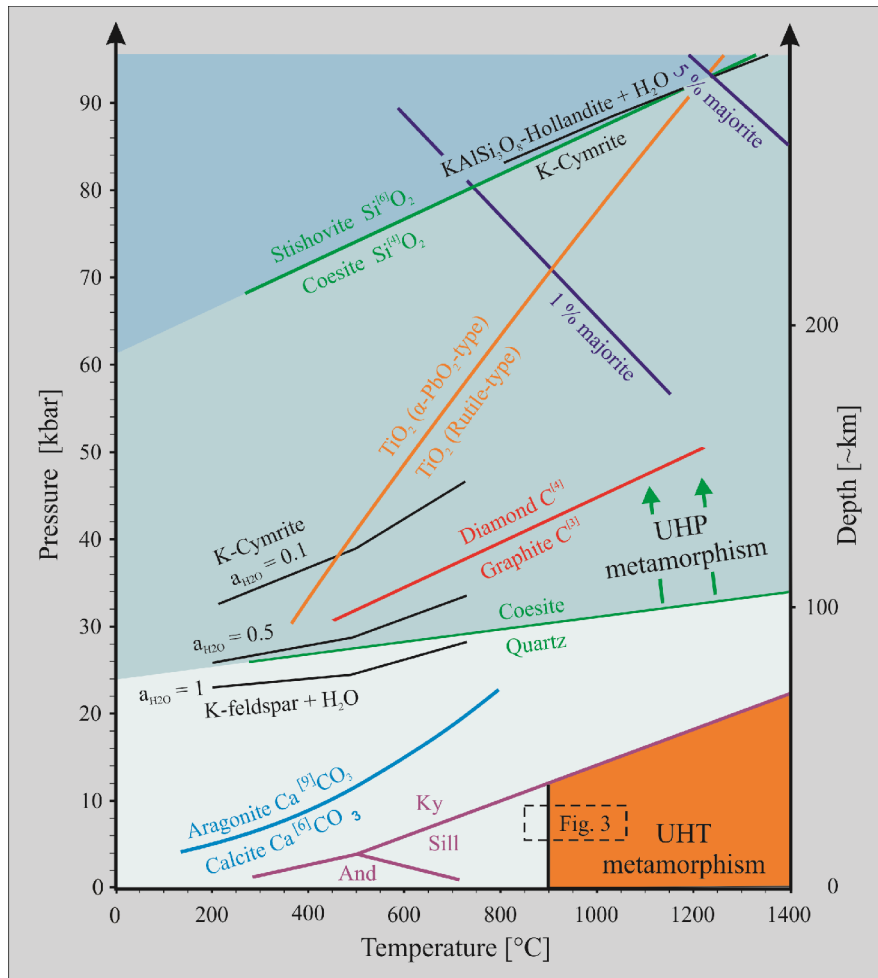
Figure 2. Pressure-temperature diagram showing the reaction boundaries for andalusite-sillimanite-kyanite (Holdaway, 1971), calcite-aragonite (Hacker et al., 2005), quartz-coesite (Bose and Ganguly, 1995), coesite-stishovite (Yong et al., 2006), graphite-diamond (Kennedy and Kennedy, 1976), rutile-type TiO_2-α-PbO_2-type TiO_2 (Kojitani et al., 2018), as well as two isopleths of majorite component in garnet (Scambelluri et al., 2008). The reaction curves K-feldspar+H_2O=K-cymrite (for water activities of 0.1, 0.5 and 1) and K-cymrite=$KAlSi_3O_8$-hollandite+H_2O are from Fasshauer et al. (1997) and Yong et al. (2006), respectively. Superscript numbers in square brackets refer to coordination numbers. The blue area above the quartz stability limit corresponds to ultrahigh-pressure metamorphism. Inset see Fig. 3.

1971), and such temperatures were later confirmed by further studies (e.g., Sandiford et al., 1987; Harley, 1985; Ellis, 1980). As a result, the term ultrahigh-temperature (UHT) metamorphism was introduced (Fig. 3) referring to granulite facies conditions exceeding 900 ºC (Harley, 1998). Whereas the upper pressure limit of UHT metamorphism was originally defined by the thermal gradient of 75 ºC/kbar, it is now defined by the sillimanite-kyanite reaction curve (Kelsey and Hand, 2015). In general, the aluminosilicate polymorphs continue to provide a useful *P-T* reference frame, particularly for those facies series with moderate to high *T/P* gradients. Furthermore, paramorphic transformations between the polymorphs can provide simple checks, albeit crude, on prograde and retrograde *P-T* trajectories (Figs. 1b, 1c).

It has been proposed that UHT metamorphic conditions can result from processes such as upwelling of hot asthenosphere, mafic intrusions, delamination processes and magmatic underplating. Furthermore, the thermal history of the Earth has to be taken into consideration, meaning that the heat content of the Earth changed with time, from the Archean to the Phanerozoic. The present mantle temperatures are interpreted to be about

200 ºC lower than 2.5 to 3 Ga ago (Herzberg et al., 2010). Classical regions of UHT-metamorphism are the Napier Complex (Antarctica), the eastern Ghats (India), the Lewisian Complex (Scotland), the Limpopo belt (Zimbabwe), Wilson Lake (Canada), the Highland Complex (Sri Lanka), the Anosyan Group (South Madagascar), and the Labwor Hills (Uganda). In Saxony, Germany, an entire mountain range, with the name "Granulitgebirge" (Granulite Mountains), exposes rocks formed under ultra-high temperatures (Hagen et al., 2008; Rötzler and Romer, 2001). The fast tectonic exhumation of this metamorphic complex generated several hundreds of meters of a contact metamorphic aureole in the hanging-wall country rock phyllites and schists (Müller et al., 2015; Reinhardt and Kleemann, 1994). According to the latest *P-T*-based classification, the granulites of Saxony are high-pressure granulites as the peak pressures are within the kyanite stability field (O'Brien and Rötzler, 2003). Nevertheless, HP granulites experiencing isothermal decompression may still pass through the UHT field, showing corresponding re-adjustments of their mineral assemblages.

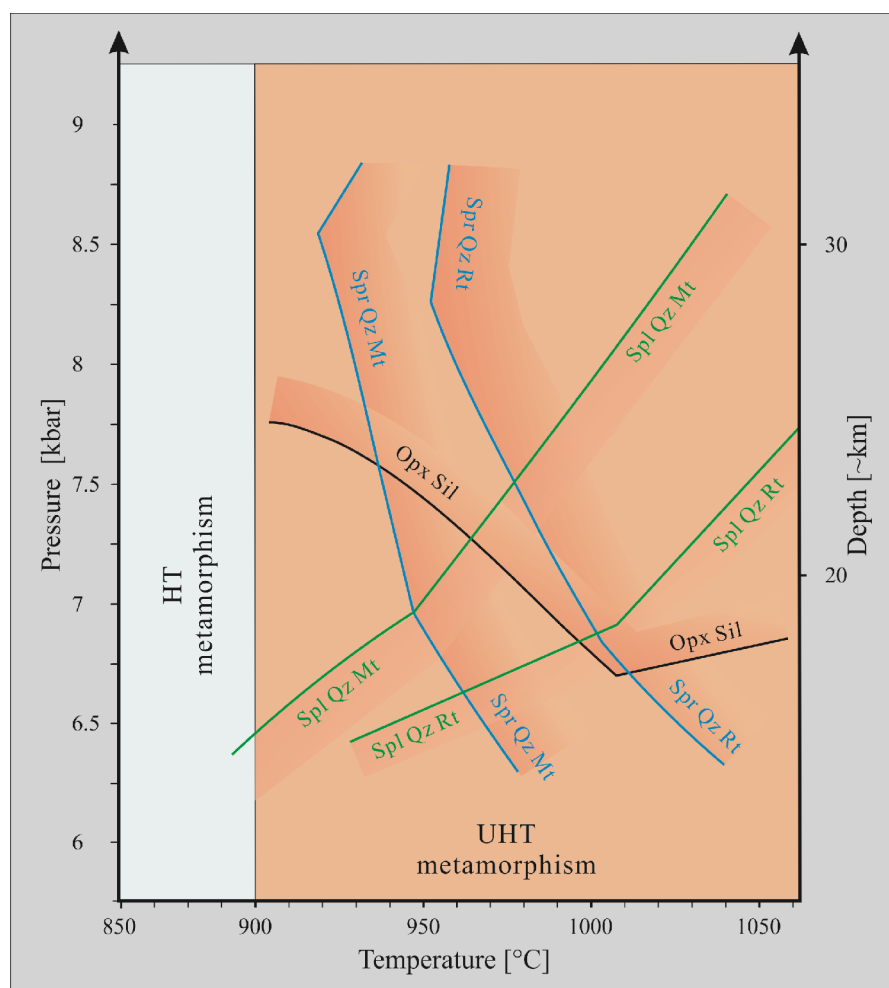Typical UHT-related assemblages for aluminous rocks

Figure 3. Lower-temperature stability limits of the assemblages sapphirine+quartz and spinel+quartz in relatively oxidized rocks (+magnetite) and relatively reduced rocks (+rutile). Sapphirine stability is shown for melt-bearing aluminous metapelites. K-feldspar and ilmenite are further excess phases. Stability limits are based on calculated univariant and invariant equilibria in the system KFMASHTO and related subsystems (after Wheller and Powell, 2014, and Kelsey and Hand, 2015). The stability limit of orthopyroxene+sillimanite is also included.

(Fig. 1d) are shown in Fig. 3. The most recent thermodynamic model presented by Wheller and Powell (2014) confirms that the assemblage sapphirine+quartz is a reliable indicator of UHT conditions in metapelitic rock compositions, while spinel+ quartz covers a larger *T* range at generally low pressures. Below the 900 ºC boundary the spinel+quartz assemblage requires extreme *T/P* gradients above 140 ºC/kbar. The stability limits of both sapphirine-quartz and spinel-quartz are strongly dependent on the oxidation state of the rock. Osumilite is considered another UHT indicator in pelitic systems, but thermodynamic data are not yet robust enough to reliably integrate this phase routinely into phase equilibrium calculations.

The findings of UHT- and UHP-metamorphic minerals and mineral assemblages generated an enormous amount of new research projects with significant implications for petrology, geodynamics, global tectonics, seismology, and geochemical recycling, and the current issue contains several contributions which focus on such topics. Metamorphism-related papers of this issue cover the entire *P-T* field; a special focus is on UHT and UHP-rocks, however. Melt intrusions into metamorphic rocks or already existing older magmatic rocks can operate as valuable markers enabling a better chronological

evaluation of events with respect to the entire evolution of an orogen. Such topics were also considered as important contributions of the current issue.

3   THE ROLE OF METASOMATISM

As a result of an interaction of aqueous or CO_2-rich fluids with rocks, chemical components may become removed or introduced, leaving behind a rock that is completely different in composition compared to its protolith.

A classical example of such a metasomatic rock is found where lenses of ultrabasic rocks are in contact with SiO_2-rich rocks such as granitic gneisses or metapelites. Along the contact monomineralic layers of talc, actinolite, chlorite and biotite can form, for example, between lenses of antigorite and a metapelitic country rock. The metasomatic rock developed along the contact is known as blackwall. Metasomatism may be due to fluid infiltration which may, for example, lead to rocks enriched in B, F, or Cl. Skarns are typically rich in Ca-silicate minerals, may contain sulfide or oxide ores, and form as a result of granitic intrusions into carbonate rocks. Furthermore, alkali-rich rocks may have a metasomatic origin (essentially Na- or K-enrichment). An example of large-scale infiltration

metasomatism is mantle metasomatism caused by fluids that are released from the downgoing slab at great depths of subduction zones and interact with minerals of the overlying mantle wedge. In the current issue, four special types of metasomatic rocks are presented: (1) sagvandite (Fig. 1e), formed by an interaction of crustal fluids and mantle rocks, (2) jadeitite (Fig. 1f), either precipitated directly from subduction zone related Na-Al-Si-rich hydrous fluids or formed by metasomatic replacement of an appropriate protolith, (3) pyrope quartzite or whiteschist (Fig. 1g) that formed from a granitic precursor by interaction with Mg-rich serpentinite-derived fluids in a subduction zone setting and (4) rodingite (Fig. 1h), which is rich in Ca, commonly sourced from the breakdown of clinopyroxene due to serpentinization of adjacent peridotite. These rocks, which typically are found as veins (Fig. 1h) and lens-like bodies in country rock lithologies, can form at different metamorphic stages during the prograde and retrograde P-T evolution, and thus their chronological interrelation with metamorphic (or magmatic) host rocks, helps to better categorize the "sequence of events" that took place during the orogen's evolution.

4   METAMORPHISM AND OROGENIC BELTS—CONTRIBUTIONS TO THIS SPECIAL ISSUE

The current special issue contains 13 papers. In this section we summarize the key messages of each contribution.

(1) Bucher and Stober (2019) present a review paper on sagvandite from the Scandinavian Caledonides. The rock essentially consists of coarse-grained radial clusters of enstatite (Fig. 1a) and magnesite and is named after its "type locality" Sagelvvatnet in northern Norway. The authors documented that sagvandite forms from dunite or harzburgite mantle fragments that were tectonically emplaced into lower crustal rocks during the Caledonian orogeny. Due to interaction of CO_2-bearing crustal fluids with the ultramafic precursors, olivine became replaced to form enstatite plus magnesite. The key reaction that occurred is $2Mg_2SiO_4+2CO_2=Mg_2Si_2O_6+2MgCO_3$. This reaction sequesters CO_2 from the fluid into solid carbonate and represents an important model reaction for planned industrial-scale CO_2 isolation. The authors showed that sagvandites are representing principal lithologies formed by an interaction of crustal fluids and mantle rocks at upper amphibolite conditions, and that they provide a better understanding of the subduction-zone-related fluid cycle and its geochemical consequences.

(2) Schertl et al. (2019) studied zircon from two metasomatic rocks, jadeitite from the Dominican Republic and pyrope quartzite from the Dora-Maira Massif and showed that core domains of zircon which were inherited from magmatic precursors may actually contain metamorphic *pseudo-inclusions*. They were not entrapped during an early stage of formation, but introduced during later metamorphic or metasomatic events along microcracks. Careful cathodoluminescence studies on zircon helped to distinguish different zircon generations and document that in case of the jadeitite, omphacite and jadeite, which were formed at ~78 Ma, are observed in 115–117 Ma magmatic oscillatory-zoned domains of zircon. In case of the pyrope quartzite, oscillatory zircon domains that document magmatic crystallization ages of ~275 Ma, contain coesite, pyrope, phengite, talc, and kyanite, formed during UHP conditions at 35 Ma. Thus,

an incautious approach to the study of mineral inclusions in zircon can lead to completely misleading interpretations of the geological context.

(3) Rodingite is a Ca-rich, Si-undersaturated rock consisting of various amounts of Ca- and Ca-Mg-silicates. In general, its formation is related to ophiolites during ocean-floor metamorphism and other hydrothermal alteration events, or the emplacement of ultramafic rocks in the continental crust. Rocks such as dolerite, gabbro, granite, greywacke and argillite, are potential protoliths of rodingite. Rodingite can also be associated with eclogite-facies rocks and may have formed prior to or after the high-pressure (HP) stage. Wang et al. (2019) focused on a suite of newly recognized rodingites from the Purang ophiolite complex, western Tibet, and performed petrological, mineral- and whole-rock geochemistry studies as well as phase equilibrium modeling. They were able to document that the studied rodingite formed in a fore-arc environment from olivine gabbro or olivine gabbronorite, by supra-subduction zone fluid infiltration at conditions of P<2 kbar and T<350–400 ºC, demonstrating that rodingites can be valuable time markers for different events relating to the emplacement of ophiolites.

(4) The Yarlung-Zangbo suture zone (YZSZ) is the main tectonic boundary between the Himalaya of the Indian Plate and the Lhasa terrane of the Asian Plate. Many ophiolite complexes that represent relics of the Neo-Tethian oceanic lithosphere prior to the collisional event are aligned along this suture zone. In their contribution Meng Y K et al. (2019) studied various types of magmatic rocks of the Zedang ophiolite and were able to chemically distinguish diabase and gabbro, which demonstrate low-K calc-alkaline and N-MORB-like characteristics, from basalt and plagiogranite with medium to high-K calc-alkaline characteristics. The authors were thus able to identify two distinct magmatic events, which could be distinguished also by zircon U-Pb dating, demonstrating that basalt and plagiogranite crystallized at about 160 Ma while gabbro was formed at ca. 131 Ma. They concluded that the early 160 Ma event indicates an intra-oceanic subduction setting followed by a younger 131 Ma event revealing an N-MORB-like setting.

(5) Willner et al. (2019) report an Early Cambrian eclogite from the Beloretsk Metamorphic Complex of the SW Urals. For the first time they provide a 7-point Rb/Sr mineral isochron (phengite, omphacite, apatite) at 532.2±9.1 Ma interpreted as age of crystallization of the eclogitic peak PT assemblage. It formed at a convergent eastern margin of Baltica during the Neoproterozoic–Early Cambrian Timanide orogeny. Similar peak P-T conditions were derived for the eclogite (16.5–18.5 kbar/525–550 ºC) and neighbouring micaschist and orthogneiss by pseudosection techniques, confirming an "*in situ*" origin. A garnet amphibolite from an overlying unit shows a similar clockwise PT loop as the eclogite, but experienced considerably lower PT conditions.

(6) During the last decade, enormous advances in analytical microbeam techniques such as LA-ICP-MS has led geoscientists to focus on fine-grained accessory minerals like zircon, monazite, rutile, titanite, apatite etc. Cao et al. (2019) used different generations of titanite and rutile of retrograde eclogite and titanite of garnet amphibolite from North Qaidam, western China, in order to get an insight into the development of the

exhumation process. They document that rutile was formed at very high pressures of 2.5–2.8 GPa and 823–884 ℃; while the granulite facies overprint occurred at 1.3–1.5 GPa and 812–894 ℃, conditions that derive from titanite-bearing breakdown products of rutile. Formation conditions of titanite in garnet amphibolite correspond to those of the granulite facies overprint. Due to additional LA-ICP-MS studies on rutile and titanite the authors were able to deduce the decompression path and also the process of melt formation during exhumation.

(7), (8) The North China Craton (NCC) can be described as a collisional amalgamation of microcontinents, ophiolites, accretionary prism and arc material, and metaclastics. In this issue, two papers are presented which focus on two localities of UHT metamorphic rocks using petrological methods including thermodynamic modeling, and U/Pb zircon geochronology. The contribution of Ma et al. (2019) focuses on pelitic granulites of the Huangtuyao area and the one of Wei et al. (2019) on mafic granulites of the Xiwangshan area, both of which belong to the Huai'an Complex of the so-called Trans-North China Orogen (TNCO) that essentially results from a collision of the Western and Eastern blocks of the NCC.

The focus of Wei et al. (2019) is on mafic granulite, which forms elongated lenses and dyke-like bodies within TTG gneisses. The authors succeeded to derive a clockwise P-T path that includes a peak metamorphic stage at 13.2–14.8 kbar and 1 050–1 080 ℃, a post-peak decompression stage at 5.7–7.3 kbar and 825–875 ℃, and a final amphibolite facies recrystallization at about 5 kbar and 660 ℃. Zircon U-Pb ages of 1 853±14 Ma were interpreted to represent the UHT stage while an age of 1 744±44 Ma is indicated to be attributed to the amphibolite facies overprint.

Ma et al. (2019) focus on pelitic granulite; they successfully compiled a clockwise P-T path, documenting a peak pressure stage at 13.8–14.1 kbar/840–850 ℃, a peak temperature UHT stage during decompression at 7–7.2 kbar/909–915 ℃ and a retrograde stage at 5 kbar/<780 ℃. Zircon U-Pb dating yields continuous age spectra from 1 976 at 51 815± 28 Ma, however on the basis of a probability density histogram, there are sufficient indications of two $^{207}Pb/^{206}Pb$ age populations at 1 951 and 1 876 Ma.

Since there is plenty of controversial discussion related to the interpretation of ages and the thermal evolution of the TNCO in general, the contributions of Wei et al. (2019) and Ma et al. (2019) represent important building blocks to gaining a deeper insight into the tectonic structure and the development of certain portions of the NCC.

(9) A detailed study on petrology, phase equilibrium modeling and U-Pb zircon ages of a metagabbro vein in peridotite from the Yushugou granulite-peridotite complex, South Tianshan (China) has been performed by Zhang et al. (2019). The authors were able to distinguish three different events. Stage I (Cpx^A+ Opx^A+Pl^A) refers to the magmatic mineral assemblage of the metagabbro vein and stage II (Cpx^B+Opx^B+Pl^B+Spl) represents the mineral assemblage of the granulite facies metamorphism at peak P-T conditions of 940–1 070 ℃ and 4.2–6.9 kbar. Stage III is characterized by the existence of prehnite, thomsonite, and amphibole in the matrix, and indicates that the metagabbro vein may have been influenced by fluids during retrograde metamor-

phism. SIMS U-Pb age dating of zircon documents that the protolith age of the metagabbro vein is 400.5±6.2 Ma, reflecting a Devonian magmatism. The granulite facies metamorphism, possibly related to post-collisional magmatism, is interpreted to have occurred at 271.5±7 Ma.

(10) Song et al. (2019) focus on U/Pb zircon- as well as Hf isotope-studies of a meta-igneous rock suite from coastal outcrops of the Liansandao area south of Huangdao (Shandong Peninsula). Protolith crystallization ages determined are 747±12 (gneissic granodiorite), 767±12 (gneissic monzodiorite) and 765±21 Ma (granitic gneiss). The rocks belong to the Sulu Orogen that is located east of the Tanlu fault, one of the major fault zones in eastern China. In the past, special emphasis was placed on the timing of the UHP metamorphism in the Sulu Orogen. However, data on the Precambrian tectono-magmatic evolution are quite scarce. The authors contribute to fill this gap by collecting further geochemical and isotope data, which indicate that metagranite and metagranodiorite likely derive from re-melting of a Paleoproterozoic continental crust and that the monzodioritic precursor formed from mantle-derived magma that interacted with the ancient continental crust.

(11) Du et al. (2019) studied porphyritic and K-feldspar granitic intrusions from the Dananhu belt, eastern Tianshan by using zircon LA-ICP-MS geochronological, whole rock major and trace element geochemistry as well as Sr-Nd isotope methods. The authors were able to determine emplacement ages of 357±3 (porphyritic granite) and 311±3 Ma (K-feldspar granite). The porphyritic granite shows geochemical and isotopic characteristics, which are similar to that of a crustal-derived magma, and is interpreted to originate from the juvenile lower crust. Some trace elements of the K-feldspar granite vary widely indicating a formation by partial melting of juvenile crust plus a considerable amount of old crustal material. The data of Du et al. (2019) support the concept that all granitoids of the Dananhu belt were emplaced in an island arc environment.

(12) The focus of Liu et al. (2019) is on Late Triassic volcanic rocks of the central Qiangtang metamorphic belt (CQMB). The locality is about 10 km south of the Chabo Lake, close to the southern margin of the CQMB. Andesite, basalt and dacite were studied using zircon U-Pb geochronology and zircon in-$situ$ Lu-Hf isotope analysis, whole rock major and trace elements as well as Sr-Nd isotope methods. Trace element patterns of basalts, andesites and dacites are essentially identical and show an enrichment in light rare earth elements (LREE) relative to heavy REE; the Eu anomalies are weakly negative to positive. Trace element compositions point to an OIB nature of all the rocks. Oscillatory zircons of a studied andesite demonstrate a magmatic age of 229.3±2.9 Ma. The volcanic rocks and related limestones observed are interpreted to represent a sequence of seamounts that was removed from the subducting Longmu Lake-Shuanghu Paleo-Tethyan oceanic slab. Other portions of seamounts have been subducted and metamorphosed at blueschist- and eclogite facies conditions.

(13) Meng F X et al. (2019) focus on eclogite and garnet clinopyroxenite xenoliths from Early Cretaceous dioritic intrusions of the North China Craton (NCC). The Xuzhou-Suzhou study area is located at the southeastern margin of the NCC, about 100 km west of the Tanlu fault and about 300 km north of

the Dabie Orogen. *P-T* estimates document the xenoliths to have formed at pressures exceeding 1.5 GPa, which corresponds to depths of >50 km. All samples define a well correlated $^{147}Sm/^{144}Nd$-$^{143}Nd/^{144}Nd$ age of 2 081 Ma, reflecting the age of the nearby granulite-facies metamorphism. They document a decoupling of the Lu-Hf and Sm-Nd isotopic systems and the Lu/Hf isochron age of 2 424 Ma is similar to the zircon age peak of the studied xenoliths and the dominant age of NCC basement, indicating an affinity of the igneous protoliths of the xenoliths to the Archean basement of the NCC. Thus, the data gained by Meng F X et al. (2019) valuable contribute to a better understanding of the development of the lower crust beneath this part of the NCC.

REFERENCES CITED

Bose, K., Ganguly, J., 1995. Quartz-Coesite Transition Revisited: Reversed Experimental Determination at 500–1 200 ℃ and Retrieved Thermochemical Properties. *American Mineralogist*, 80(3/4): 231–238. https://doi.org/10.2138/am-1995-3-404

Bucher, K., Stober, I., 2019. Interaction of Mantle Rocks with Crustal Fluids: Sagvandites of the Scandinavian Caledonides. *Journal of Earth Science*, 30(6): 1084–1094. https://doi.org/10.1007/s12583-019-1257-2

Cao, Y. T., Liu, L., Yang, W. Q., et al., 2019. Reconstruction the Process of Partial Melting of the Retrograde Eclogite from the North Qaidam, Western China: Constraints from Titanite U-Pb Dating and Mineral Chemistry. *Journal of Earth Science*, 30(6): 1166–1177. https://doi.org/10.1007/s12583-019-1253-6

Chopin, C., 1984. Coesite and Pure Pyrope in High-Grade Blueschists of the Western Alps: A First Record and Some Consequences. *Contributions to Mineralogy and Petrology*, 86(2): 107–118

Du, L., Yuan, C., Li, X.-P., et al., 2019. Petrogenesis and Geodynamic Implications of the Carboniferous Granitoids in the Dananhu Belt, Eastern Tianshan Orogenic Belt. *Journal of Earth Science*, 30(6): 1243–1252. https://doi.org/10.1007/s12583-019-1256-3

Ellis, D. J., 1980. Osumilite-Sapphirine-Quartz Granulites from Enderby Land, Antarctica: *P-T* Conditions of Metamorphism, Implications for Garnet-Cordierite Equilibria and the Evolution of the Deep Crust. *Contributions to Mineralogy and Petrology*, 74(2): 201–210

Fasshauer, D. W., Chatterjee, N. D., Marler, B., 1997. Synthesis, Structure, Thermodynamic Properties, and Stability Relations of K-Cymrite, $K[AlSi_3O_8]\cdot H_2O$. *Physics and Chemistry of Minerals*, 24(6): 455–462. https://doi.org/10.1007/s002690050060

Hacker, B. R., Rubie, D. C., Kirby, S. H., et al., 2005. The Calcite→

Aragonite Transformation in Low-Mg Marble: Equilibrium Relations, Transformation Mechanisms, and Rates. *Journal of Geophysical Research*, 110(B3): B03205. https://doi.org/10.1029/2004jb003302

Hagen, B., Hoernes, S. R., Rötzler, J., 2008. Geothermometry of the Ultrahigh-Temperature Saxon Granulites Revisited. Part II: Thermal Peak Conditions and Cooling Rates Inferred from Oxygen-Isotope Fractionations. *European Journal of Mineralogy*, 20(6): 1117–1133. https://doi.org/10.1127/0935-1221/2008/0020-1858

Harley, S. L., 1985. Garnet-Orthopyroxene Bearing Granulites from Enderby Land, Antarctica: Metamorphic Pressure Temperature-Time Evolution of the Archaean Napier Complex. *Journal of Petrology*, 26(4): 819–856. https://doi.org/10.1093/petrology/26.4.819

Harley, S. L., 1998. On the Occurrence and Characterization of Ultrahigh-Temperature Crustal Metamorphism. *Geological Society, London, Special Publications*, 138(1): 81–107. https://doi.org/10.1144/gsl.sp.1996.138.01.06

Herzberg, C., Condie, K., Korenaga, J., 2010. Thermal History of the Earth and Its Petrological Expression. *Earth and Planetary Science Letters*, 292(1/2): 79–88. https://doi.org/10.1016/j.epsl.2010.01.022

Holdaway, M. J., 1971. Stability of Andalusite and the Aluminum Silicate Phase Diagram. *American Journal of Science*, 271(2): 97–131. https://doi.org/10.2475/ajs.271.2.97

Kelsey, D. E., Hand, M., 2015. On Ultrahigh Temperature Crustal Metamorphism: Phase Equilibria, Trace Element Thermometry, Bulk Composition, Heat Sources, Timescales and Tectonic Settings. *Geoscience Frontiers*, 6(3): 311–356. https://doi.org/10.1016/j.gsf.2014.09.006

Kennedy, C. S., Kennedy, G. C., 1976. The Equilibrium Boundary between Graphite and Diamond. *Journal of Geophysical Research*, 81(14): 2467–2470. https://doi.org/10.1029/jb081i014p02467

Kojitani, H., Yamazaki, M., Kojima, M., et al., 2018. Thermodynamic Investigation of the Phase Equilibrium Boundary between TiO_2 Rutile and Its α-PbO_2-Type High-Pressure Polymorph. *Physics and Chemistry of Minerals*, 45(10): 963–980. https://doi.org/10.1007/s00269-018-0977-7

Liu, D. L., Shi, R. D., Ding, L., et al., 2019. Survived Seamount Reveals an *in situ* Origin for the Central Qiangtang Metamorphic Belt in the Tibetan Plateau. *Journal of Earth Science*, 30(6): 1253–1265. https://doi.org/10.1007/s12583-019-1250-9

Liu, L., Zhang, J. F., Green, H. W. II, et al., 2007. Evidence of Former Stishovite in Metamorphosed Sediments, Implying Subduction to >350 km. *Earth and Planetary Science Letters*, 263(3/4): 180–191. https://doi.org/10.1016/j.epsl.2007.08.010

Ma, S. T., Li, X.-P., Liu, H., et al., 2019. Ultrahigh Temperature Metamorphic Record of Pelitic Granulites in the Huangtuyao Area of the Huai'an Complex, North China Craton. *Journal of Earth Science*, 30(6): 1178–1196. https://doi.org/10.1007/s12583-019-1245-6

Meng, F. X., Xu, W. L., Xu, Q. L., et al., 2019. Decoupling of Lu-Hf and Sm-Nd Isotopic Systems in Deep-Seated Xenoliths from the Xuzhou-Suzhou Area, China: Differences in Element Mobility during Metamorphism. *Journal of Earth Science*, 30(6): 1266–1279. https://doi.org/10.1007/s12583-019-1255-4

Meng, Y. K., Xiong, F. H., Yang, J. S., et al., 2019. Tectonic Implications and Petrogenesis of the Various Types of Magmatic Rocks from the Zedang Area in Southern Tibet. *Journal of Earth Science*, 30(6): 1125–1143. https://doi.org/10.1007/s12583-019-1248-3

Morse, S. A., Talley, J. H., 1971. Sapphirine Reactions in Deep-Seated Granulites near Wilson Lake, Central Labrador, Canada. *Earth and Planetary Science Letters*, 10(3): 325–328. https://doi.org/10.1016/0012-821x(71)90037-9

Müller, T., Massonne, H. J., Willner, A. P., 2015. Timescales of Exhumation

and Cooling Inferred by Kinetic Modeling: An Example Using a La-mellar Garnet Pyroxenite from the Variscan Granulitgebirge, Germany. *American Mineralogist*, 100(4): 747–759. https://doi.org/10.2138/am-2015-4946

O'Brien, P. J., Rötzler, J., 2003. High-Pressure Granulites: Formation, Recovery of Peak Conditions and Implications for Tectonics. *Journal of Metamorphic Geology*, 21(1): 3–20. https://doi.org/10.1046/j.1525-1314.2003.00420.x

Reinhardt, J., Kleemann, U., 1994. Extensional Unroofing of Granulitic Lower Crust and Related Low-Pressure, High-Temperature Metamorphism in the Saxonian Granulite Massif, Germany. *Tectonophysics*, 238(1/2/3/4): 71–94. https://doi.org/10.1016/0040-1951(94)90050-7

Rötzler, J., Romer, R. L., 2001. *P-T-t* Evolution of Ultrahigh-Temperature Granulites from the Saxon Granulite Massif, Germany. Part I: Petrology. *Journal of Petrology*, 42(11): 1995–2013. https://doi.org/10.1093/petrology/42.11.1995

Sandiford, M., Neall, F. B., Powell, R., 1987. Metamorphic Evolution of Aluminous Granulites from Labwor Hills, Uganda. *Contributions to Mineralogy and Petrology*, 95(2): 217–225. https://doi.org/10.1007/bf00381271

Scambelluri, M., Pettke, T., van Roermund, H. L. M., 2008. Majoritic Garnets Monitor Deep Subduction Fluid Flow and Mantle Dynamics. *Geology*, 36(1): 59–62. https://doi.org/10.1130/g24056a.1

Schertl, H.-P., Hertwig, A., Maresch, W. V., 2019. Cathodoluminescence Microscopy of Zircon in HP- and UHP-Metamorphic Rocks: A Fundamental Technique for Assessing the Problem of Inclusions versus *Pseudo-Inclusions*. *Journal of Earth Science*, 30(6): 1095–1107. https://doi.org/10.1007/s12583-019-1246-5

Smith, D. C., 1984. Coesite in Clinopyroxene in the Caledonides and Its Implications for Geodynamics. *Nature*, 310(5979): 641–644. https://doi.org/10.1038/310641a0

Sobolev, N. V., Shatsky, V. S., 1990. Diamond Inclusions in Garnets from Metamorphic Rocks: A New Environment for Diamond Formation. *Nature*, 343(6260): 742–746. https://doi.org/10.1038/343742a0

Song, Z. J., Liu, H. M., Meng, F. X., et al., 2019. Zircon U-Pb Ages and Hf Isotopes of Neoproterozoic Meta-Igneous Rocks in the Liansandao Area, Northern Sulu Orogen, Eastern China, and the Tectonic Implications. *Journal of Earth Science*, 30(6): 1230–1242. https://doi.org/10.1007/s12583-019-1252-7

Wang, S. J., Li, X.-P., Duan, W. Y., et al., 2019. Record of Early-Stage Rodingitization from the Purang Ophiolite Complex, Western Tibet. *Journal of Earth Science*, 30(6): 1108–1124. https://doi.org/10.1007/s12583-019-1244-7

Wei, G. D., Kong, F. M., Liu, H., et al., 2019. Petrology, Metamorphic *P-T* Paths and Zircon U-Pb Ages for Paleoproterozoic Mafic Granulites from Xuanhua Complex, North China Craton. *Journal of Earth Science*, 30(6): 1197–1214. https://doi.org/10.1007/s12583-019-1251-8

Wheller, C. J., Powell, R., 2014. A New Thermodynamic Model for Sapphirine: Calculated Phase Equilibria in K_2O-FeO-MgO-Al_2O_3-SiO_2-H_2O-TiO_2-Fe_2O_3. *Journal of Metamorphic Geology*, 32(3): 287–299. https://doi.org/10.1111/jmg.12067

Whitney, D. L., Evans, B. W., 2010. Abbreviations for Names of Rock-Forming Minerals. *American Mineralogist*, 95(1): 185–187. https://doi.org/10.2138/am.2010.3371

Willner, A. P., Gopon, M., Glodny, J., et al., 2019. Timanide (Ediacaran–Early Cambrian) Metamorphism at the Transition from Eclogite to Amphibolite Facies in the Beloretsk Complex, SW-Urals, Russia. *Journal of Earth Science*, 30(6): 1144–1165. https://doi.org/10.1007/s12583-019-1249-2

Yong, W. J., Dachs, E., Withers, A. C., et al., 2006. Heat Capacity and Phase Equilibria of Hollandite Polymorph of $KAlSi_3O_8$. *Physics and Chemistry of Minerals*, 33(3): 167–177. https://doi.org/10.1007/s00269-006-0063-4

Zhang, L., Zhu, J. J., Xia, B., et al., 2019. Metamorphism and Zircon Geochronological Studies of Metagabbro Vein in the Yushugou Granulite-Peridotite Complex from South Tianshan, China. *Journal of Earth Science*, 30(6): 1215–1229. https://doi.org/10.1007/s12583-019-1254-5